Appendix for

The complete structure of the chloroplast 70S ribosome in complex with translation factor pY

Philipp Bieri, Marc Leibundgut, Martin Saurer, Daniel Boehringer, Nenad Ban*

* Corresponding author. E-mail: ban@mol.biol.ethz.ch

This file contains:

Appendix Figures S1-S12

Appendix Tables S1-S4

Additional References

Appendix Figures S1-S12

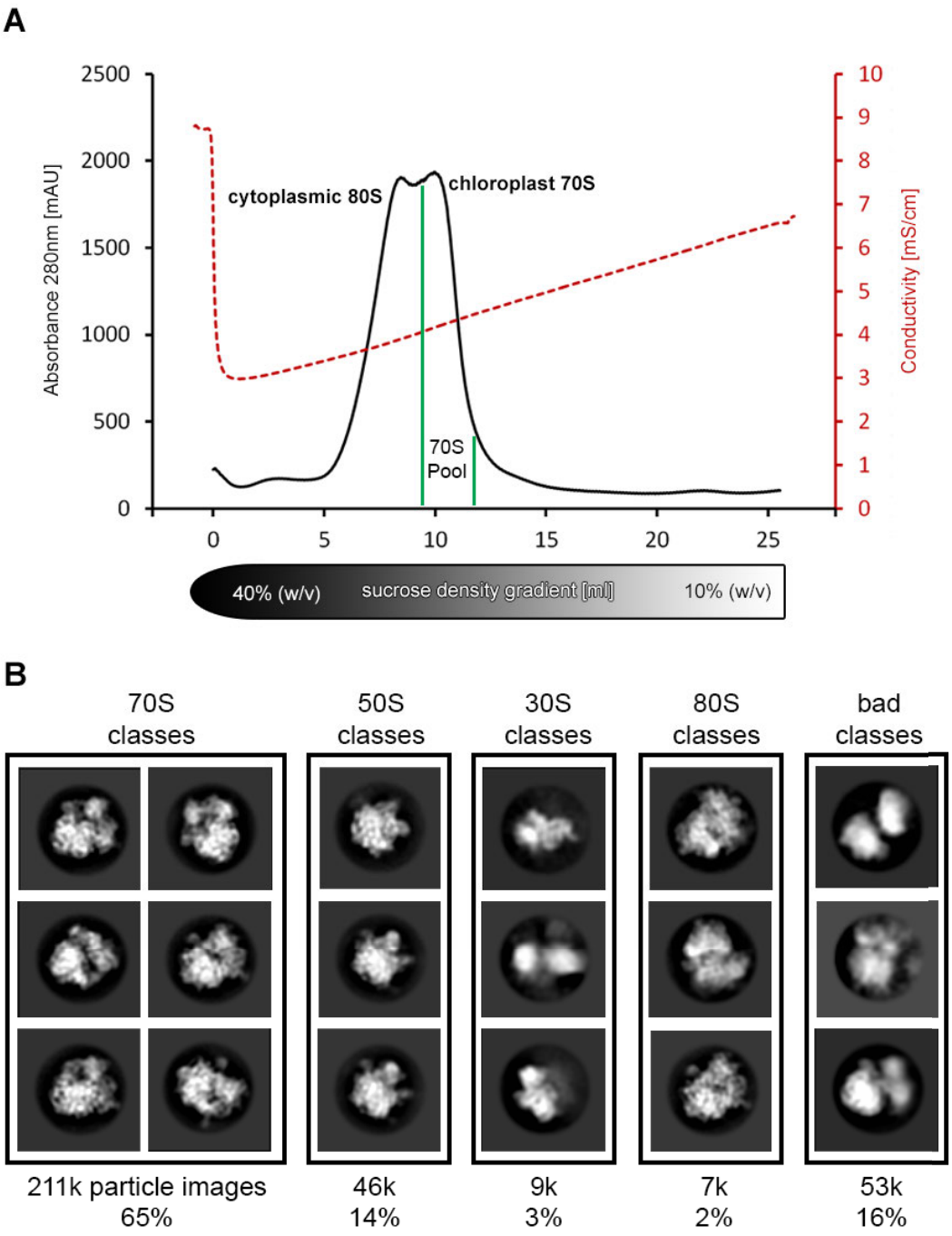

Figure S1. Purification of chloroplast 70S ribosomes. (**A**) Separation of chloroplast 70S ribosomes from cytoplasmic 80S ribosomes by sucrose density gradient centrifugation. The absorbance at 280 nm of the ribosome sample purified from spinach leaves is shown as black curve. The chloroplast 70S fraction harvested for structure determination is indicated with green lines. (**B**) Selection of 2D class averages. In the initial 2D classification performed with RELION, total 326'094 particles were sorted into 200 classes and 211'146 particles (65%) assigned to the chloroplast 70S ribosomes subset were selected for further 3D classifications and high resolution refinement steps. Particles (2%) assigned to class averages indicating cytoplasmic 80S ribosome form a minor subpopulation of the total picked particles and were removed together with particle images from the 50S, 30S and bad classes. The number of particles and the percentage from the total picked particles (326k) for each type of particle subset (70S, 50S, 30S, 80S, and bad) are indicated.

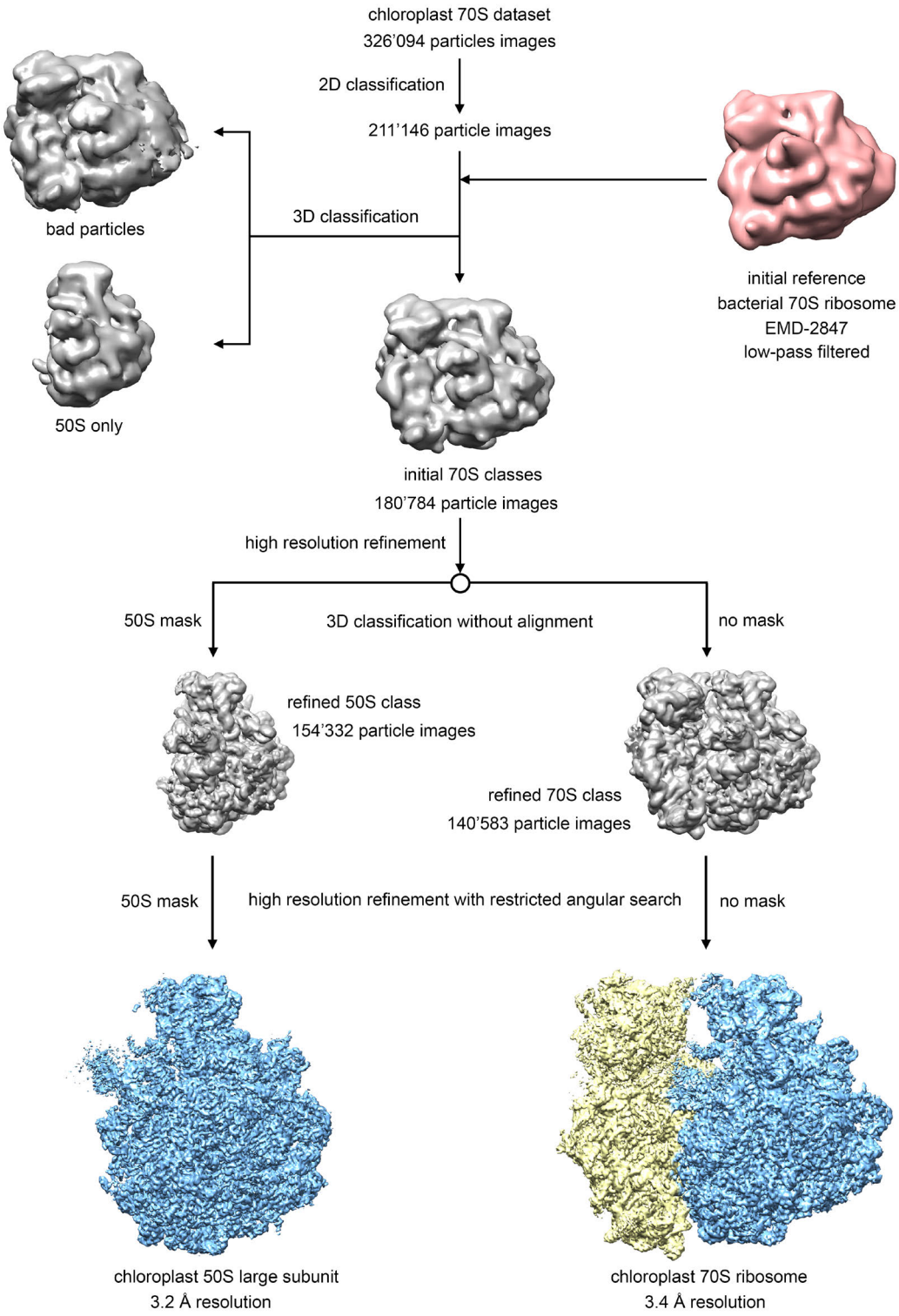

Figure S2. Computational sorting of the dataset for determination of the plastid 70S ribosome and the 50S subunit cryo-EM maps. After initial 2D and 3D classification with binned particle images, the full-size particle images (1.39 Å/px on the object scale, 320 px frame size) were refined without or by applying a mask, respectively. To further remove misaligned and lower quality particles, a second 3D classification with full-size particle images was performed in RELION by skipping the alignment procedure. The resulting subpopulation of particle images assigned to 70S classes (140'583 particle images) and 50S classes (154'332 particle images) were refined to high resolution in RELION using limited angular searches, full-size images and by applying no mask or a mask around the large subunit, respectively.

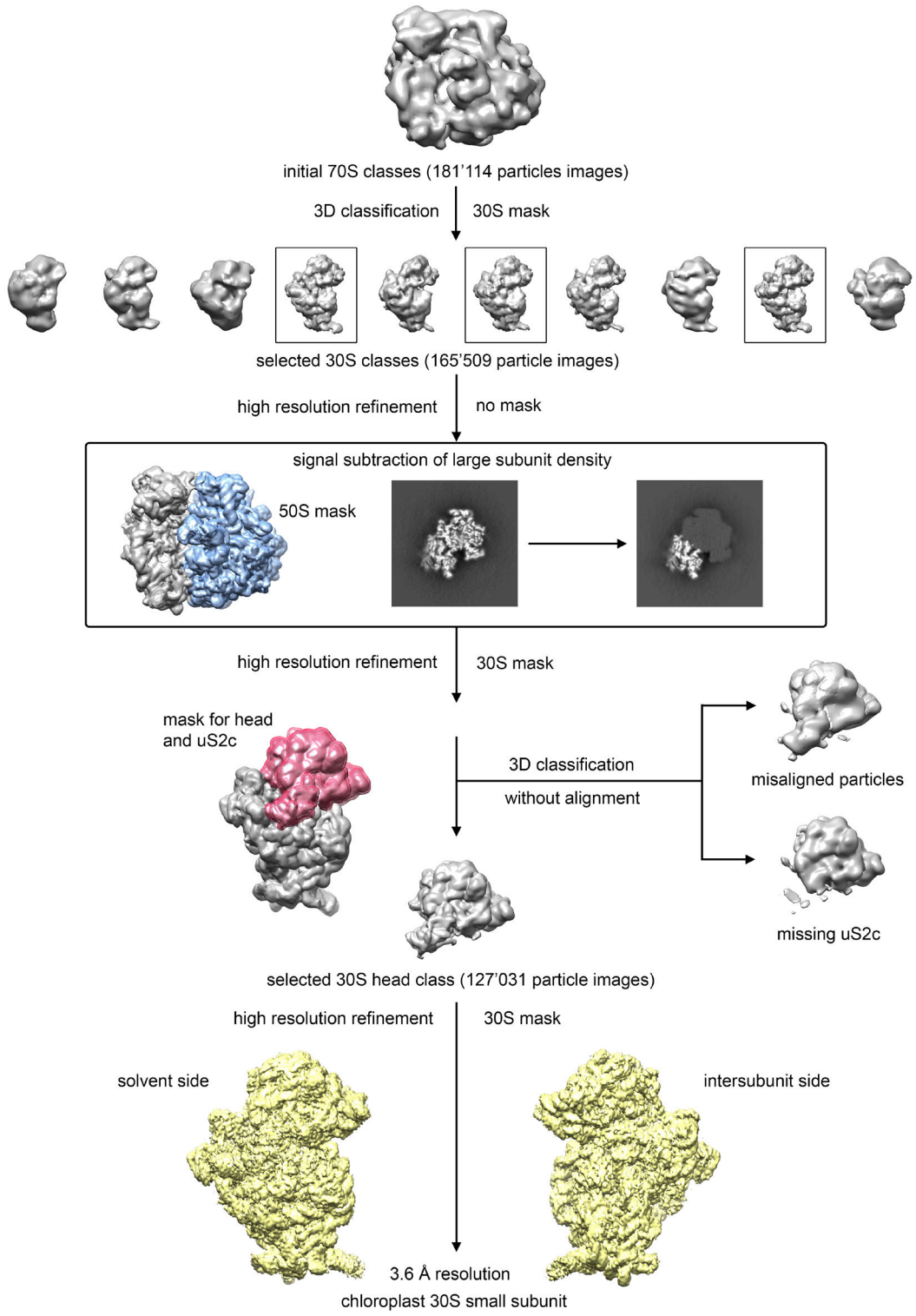

Figure S3. Computational sorting of the dataset for determination the 30S subunit cryo-EM map. Because the 30S small subunit showed more structural flexibility, further classification and signal subtraction approaches have been applied to obtain a more homogenous particle dataset and to improve the alignment of the particle images. Initially selected 70S particles (181’114 particle images) were subjected to an additional 3D classification using the binned particle images (5.56 Å/px on the object scale, 80 px frame size) with a mask applied to the 30S subunit. The subpopulation of selected 30S classes (165’509 particle images) was refined at full pixel-size without applying a mask. The resulting 70S map and aligned particle images were used for signal subtraction (Bai et al., 2015) of the large subunit from the experimental data. Therefore, a tight mask around the large subunit was applied to the 70S map and the resulting 50S density was subtracted from the aligned particle images. The signal subtracted particles were aligned to the 30S subunit by a high resolution refinement. Because

the initial 3D classification for the small subunit showed partial occupancy of bS1c and uS2c at the platform and slight movement of the head, the aligned signal subtracted particle images were subjected to a 3D classification by applying a mask around the head and bS1c/uS2c/uS5c-density. Misaligned or degraded particles and particles missing density for bS1c and uS2c were removed. With the resulting particle subpopulation (127’073 particle images), the final high resolution refinement with the full-size particle images and a 30S mask was performed.

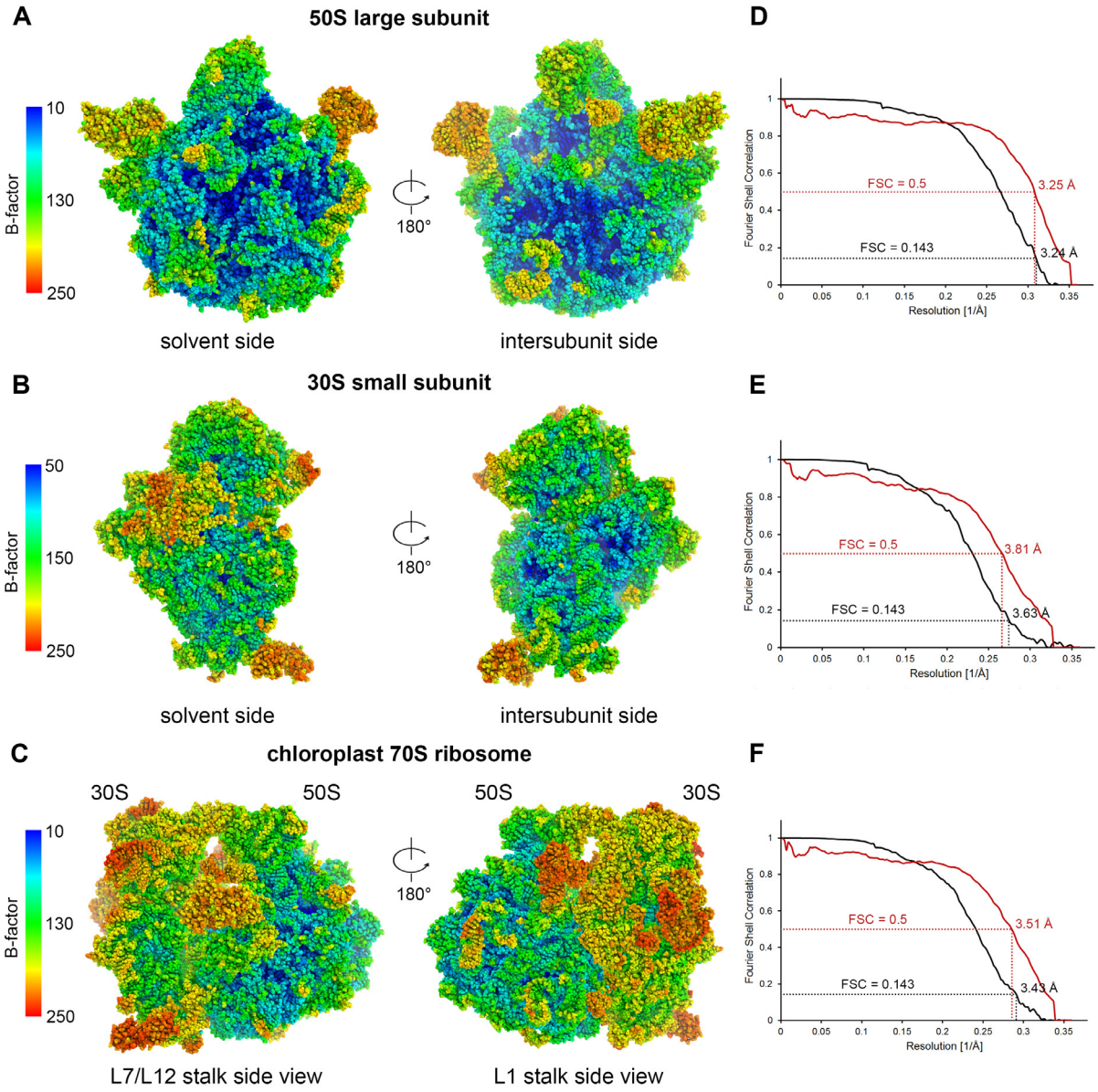

Figure S4. Coordinate refinement of the atomic models. (A-C) B-factor distribution in the atomic models of the 50S subunit (A), the 30S subunit (B), and the complete 70S ribosome (C). **(D-F)** Refinement validation. Black: Fourier Shell Correlation (FSC) curve of the 50S (D), 30S (E), and 70S map (F) with estimated resolution of 3.2 Å, 3.6 Å, and 3.4 Å, respectively, according to the FSC=0.143 criterion. Red: FSC curve computed from the final cryo-EM map and the refined atomic coordinates. In this case, the FSC=0.5 criterion was used for the validation of the atomic coordinate refinement.

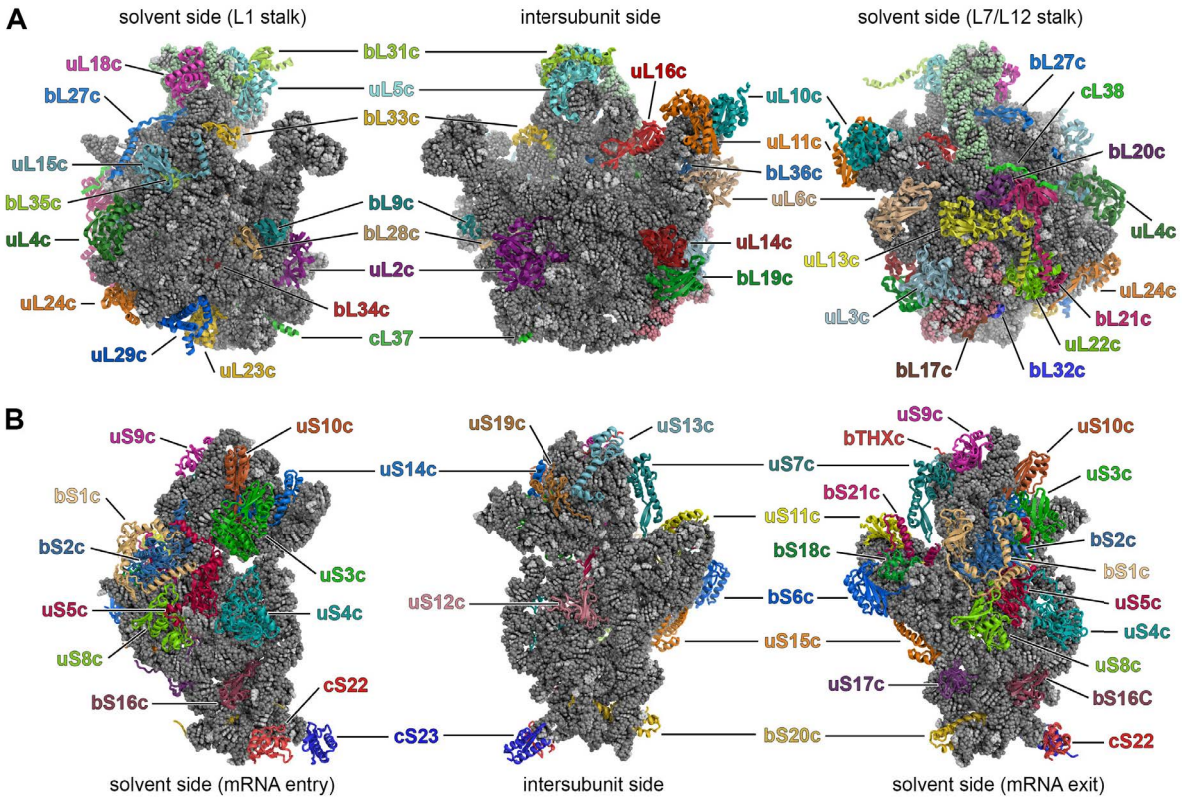

Figure S5. Ribosomal proteins of the chloroplast 70S ribosome. (**A-B**) The ribosomal proteins of the 50S large subunit (A) and of the 30S small subunit (B) are indicated with different colours. The ribosomal RNA elements are shown as spheres (50S subunit: 23S rRNA in grey, 5S rRNA in green, and 4.5S rRNA in red; 30S subunit: 16S rRNA in grey).

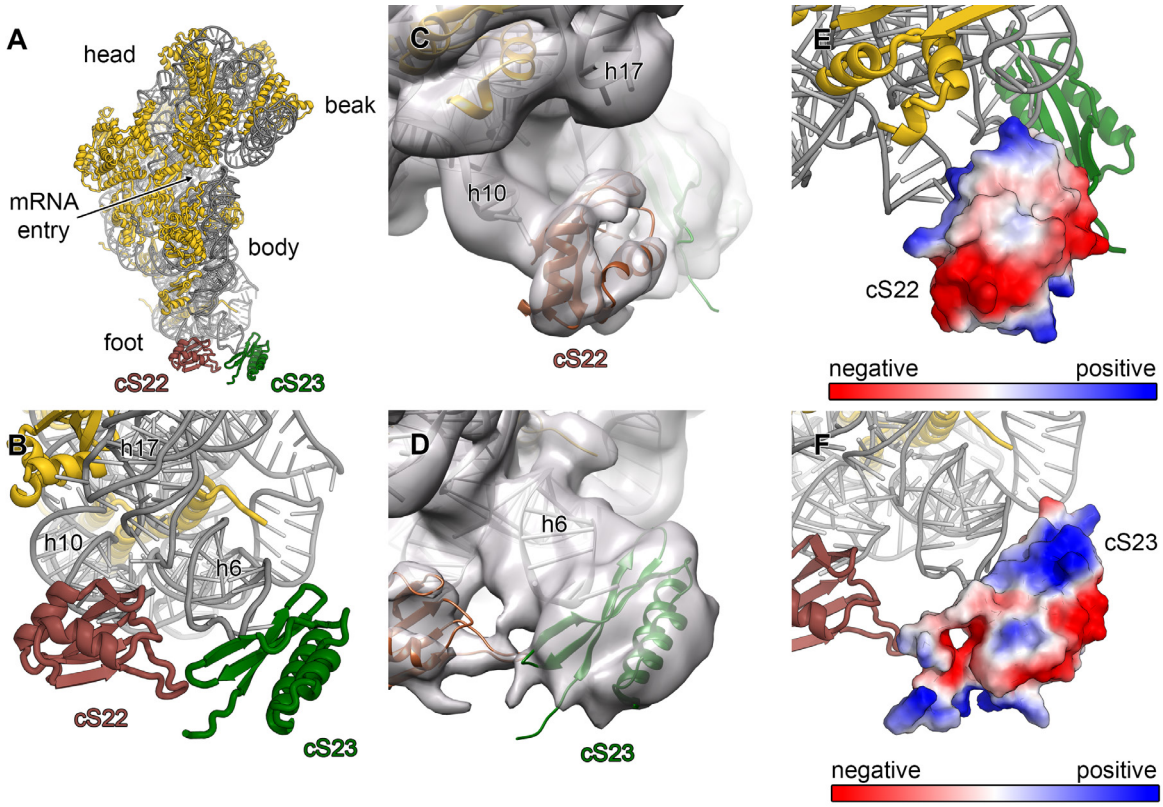

Figure S6. Rigid body fit of plastid-specific ribosomal proteins cS22 and cS23. (**A-B**) 30S subunit view from the mRNA entry site. The plastid-specific ribosomal proteins, cS22 (maroon) and cS23 (green), are bound to the foot of the 30S subunit. (**C-D**) Rigid body fit of the homology models of cS22 (C) and cS23 (D) into a low-pass filtered cryo-EM map. (**E-F**) Surface potential representation of cS22 (E) and cS23 (F). Negatively charged residues are mainly pointing towards the solvent. The interaction with the rRNA is mediated by positively charged residues, which contact the rRNA backbone, or by hydrophobic residues, which interact with the rRNA bases.

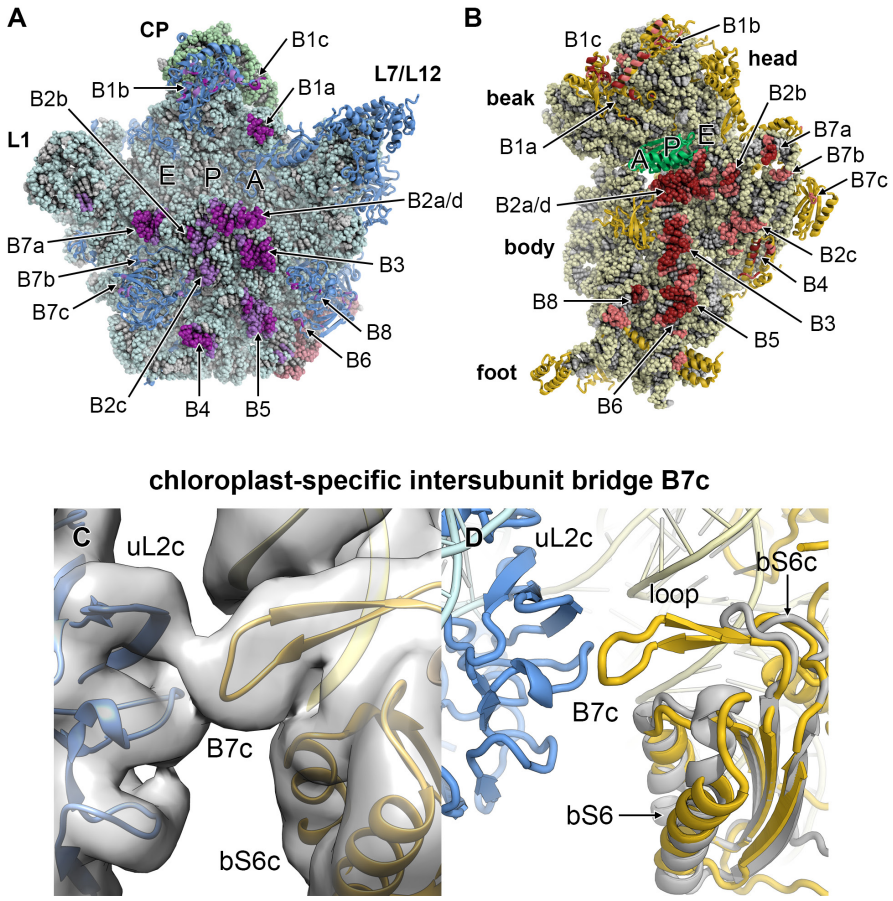

Figure S7. Intersubunit bridges. (**A**-**B**) Intersubunit bridges in the non-rotated (pY-bound) state of the chloroplast 70S ribosome. The 50S subunit (A) and the 30S subunit (B) are shown from the subunit interface side. Contact surfaces (distance <4 Å) and surfaces in close proximity (<6 Å) are coloured in purple and pale purple (A) or red and pale red (B), respectively. The names of the intersubunit bridges are indicated. (**C**-**D**) Chloroplast-specific intersubunit bridge B7c. The contact between uL2c (blue) of the 50S subunit and bS6c (yellow) of the 30S subunit are revealed by the cryo-EM reconstruction (C). For better visualization, a low-pass filter to 6 Å was applied to the 70S map. In panel D, bacterial bS6 (grey) from a 70S crystal structure (PDB 4YBB, (Noeske et al., 2015)) is overlaid. The loop of bS6c contacting uL2c and thereby forming the intersubunit bridge B7c is significantly shorter in bacterial ribosomes.

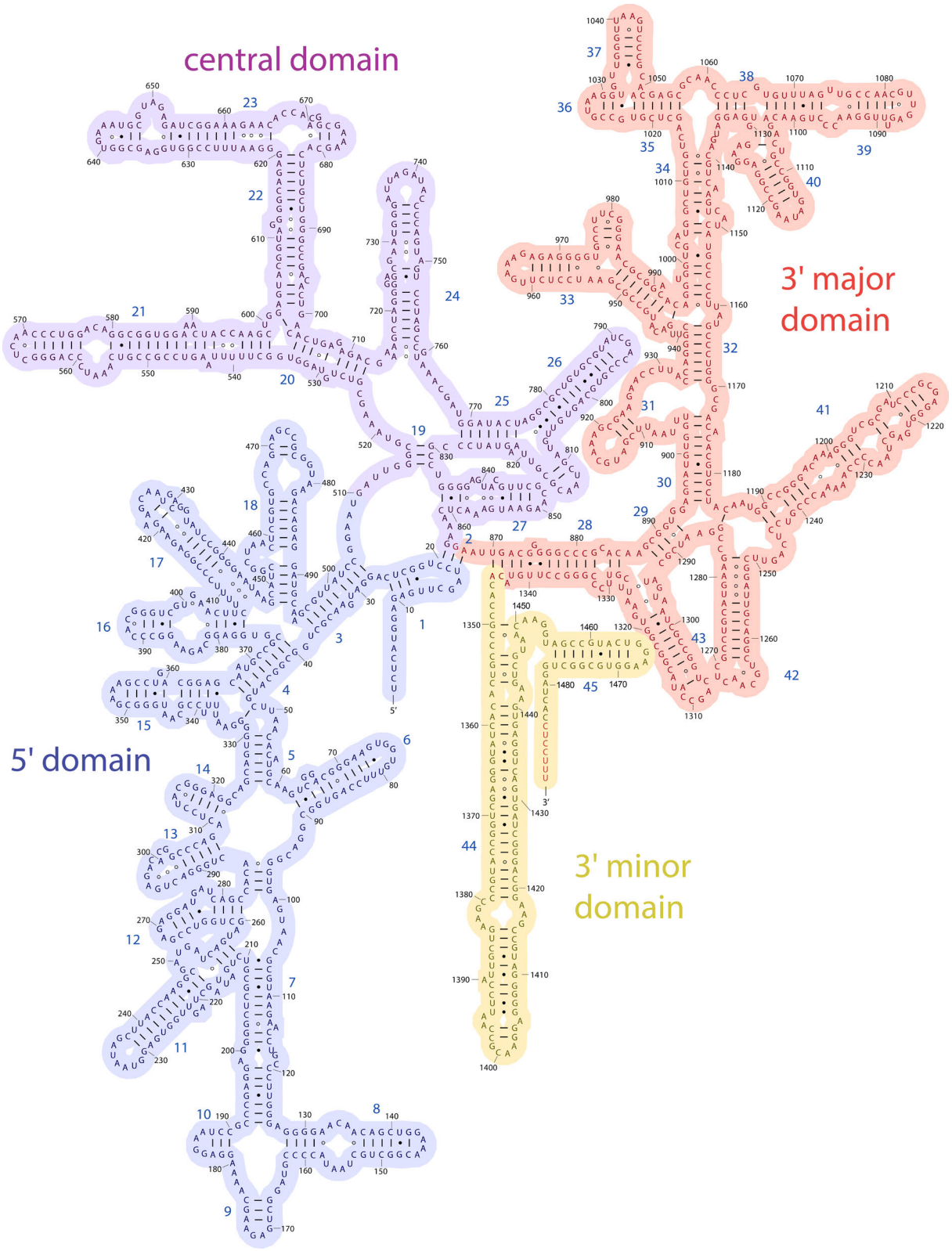

Figure S8. Secondary structure diagram of the small ribosomal subunit rRNA element. The domains of the 16S rRNA are labelled and delineated in colour. Nucleotides not built in our structure are printed in red. Watson-Crick base pairs are indicated by lines (–), G●U base pairs by dots (●), and nonstandard base pairs by rings (○). The depiction is based on the secondary structure diagram of bacterial 16S rRNA (Yusupov et al., 2001) and the template was obtained from the Noller lab web page http://rna.ucsc.edu/rnacenter/noller_lab.html.

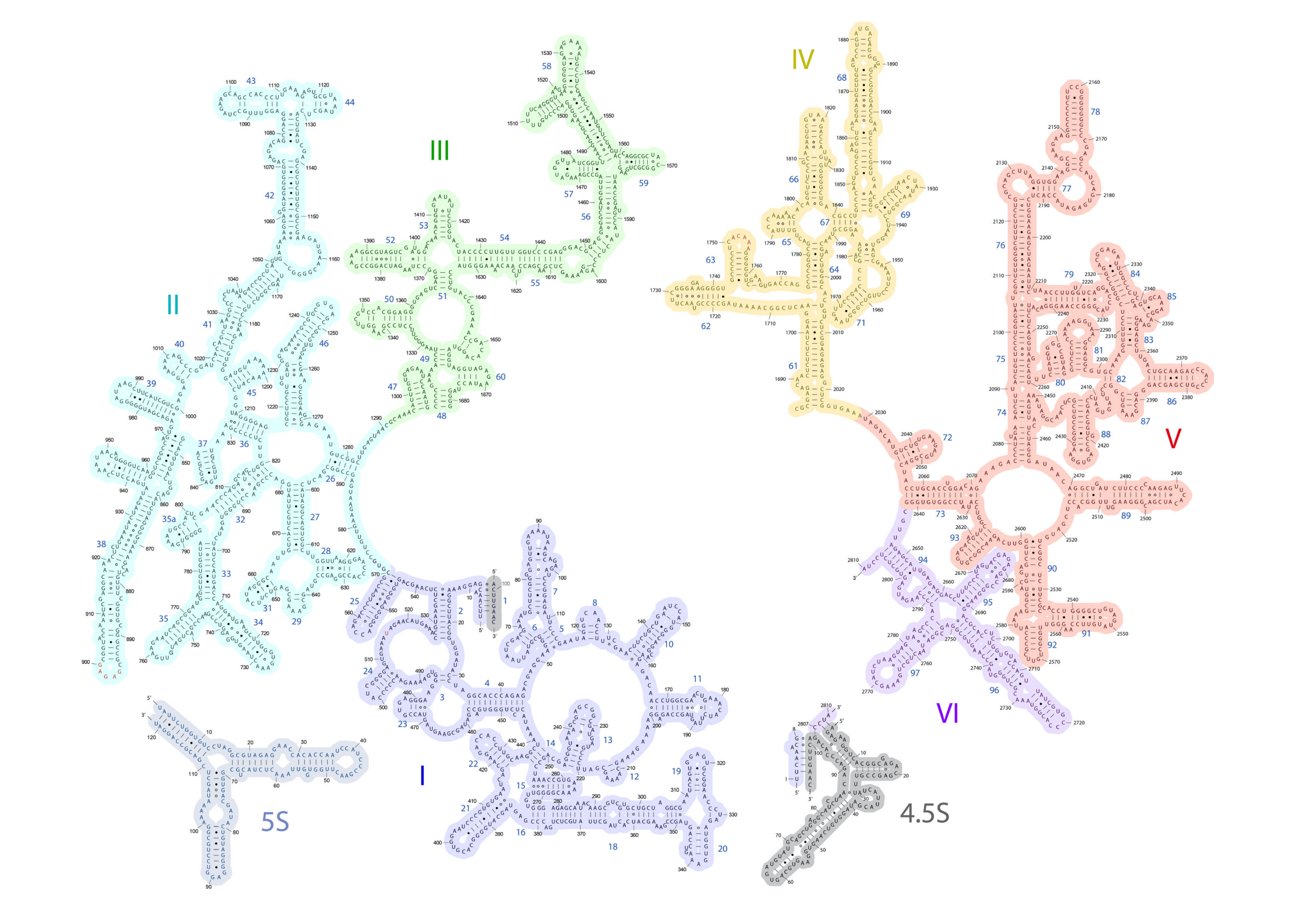
I
II
III
IV
V
VI
5S
4.5S

Figure S9. Secondary structure diagrams of the large ribosomal subunit rRNA elements. The 5S rRNA, 4.5S rRNA, and the domains of the 23S rRNA are labelled and delineated in colour. Nucleotides not built in our structure are printed in red. Watson-Crick base pairs are indicated by lines (–), G●U base pairs by dots (●), and nonstandard base pairs by rings (○). The depiction is based on the secondary structure diagram of the bacterial 23S rRNA and the 5S rRNA (Yusupov et al., 2001) and the templates were obtained from the Noller lab web page http://rna.ucsc.edu/rnacenter/noller_lab.html.

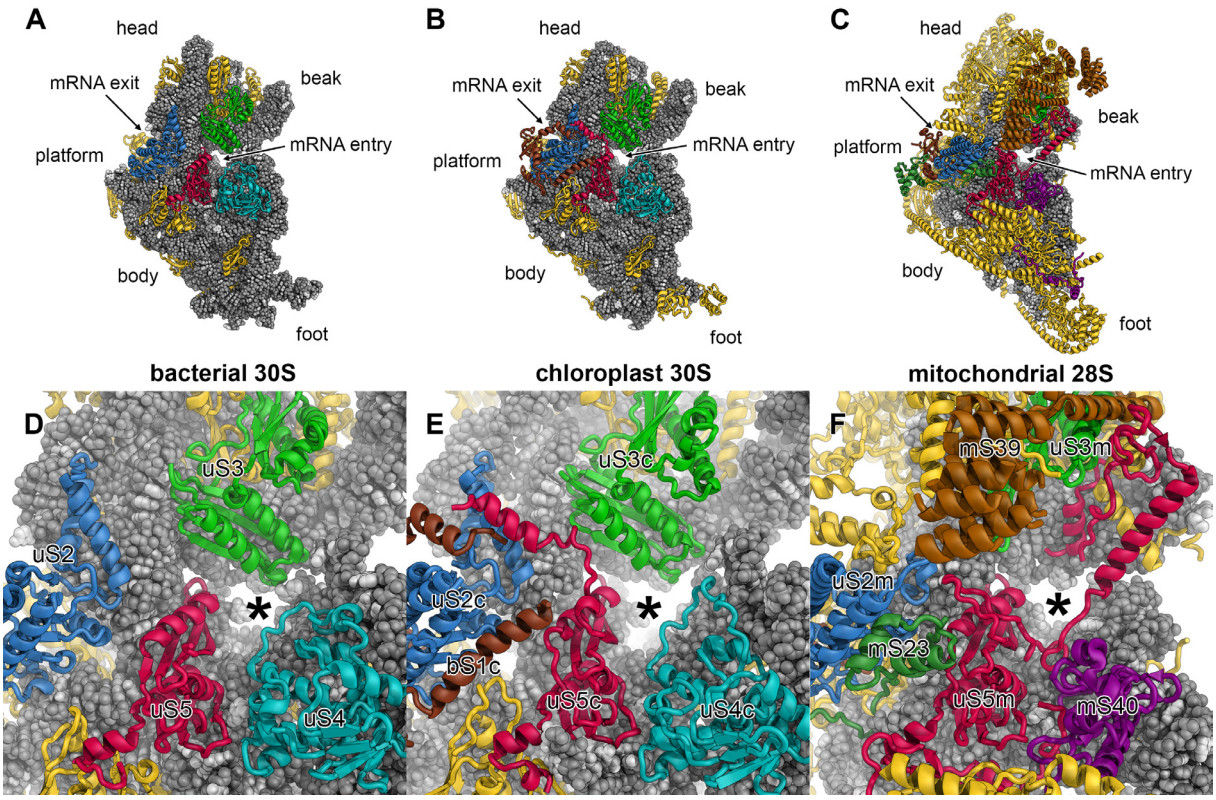

Figure S10. Comparison of the mRNA entry site between the bacterial, the chloroplast, and the mitochondrial small ribosomal subunits. (**A-C**) The bacterial 30S subunit (PDB 4YBB, (Noeske et al., 2015)) (A), the chloroplast 30S subunit (B), and the mammalian mitochondrial 28S subunit (PDB 5AJ3, (Greber et al., 2015)) (C) are shown from the solvent side. (**D-F**) Enlarged views of A, B, and C. The mRNA entry site is marked with an asterisk.

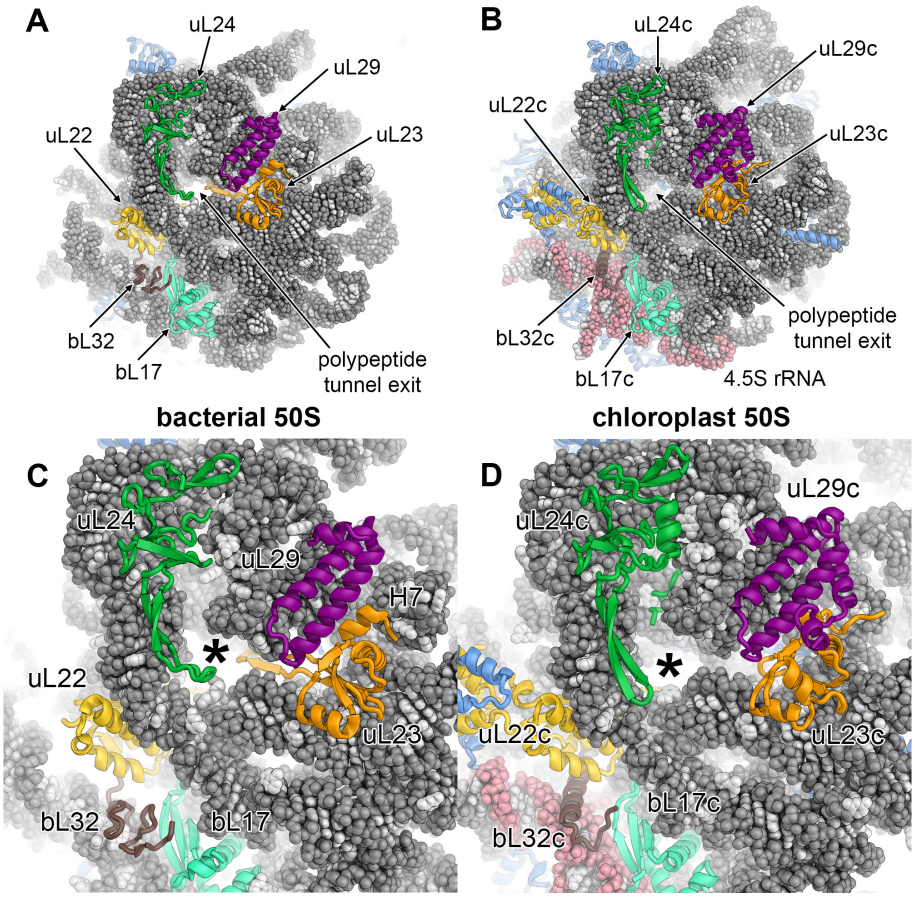

Figure S11. Comparison of the polypeptide tunnel exit between the bacterial and the chloroplast large ribosomal subunits. (**A-B**) Views showing the polypeptide tunnel exit of the bacterial 50S subunit (PDB 4YBB, (Noeske et al., 2015)) (A) and of the chloroplast 50S subunit (B). (**C-D**) Enlarged views of panels A and B. The polypeptide tunnel exit is marked with an asterisk.

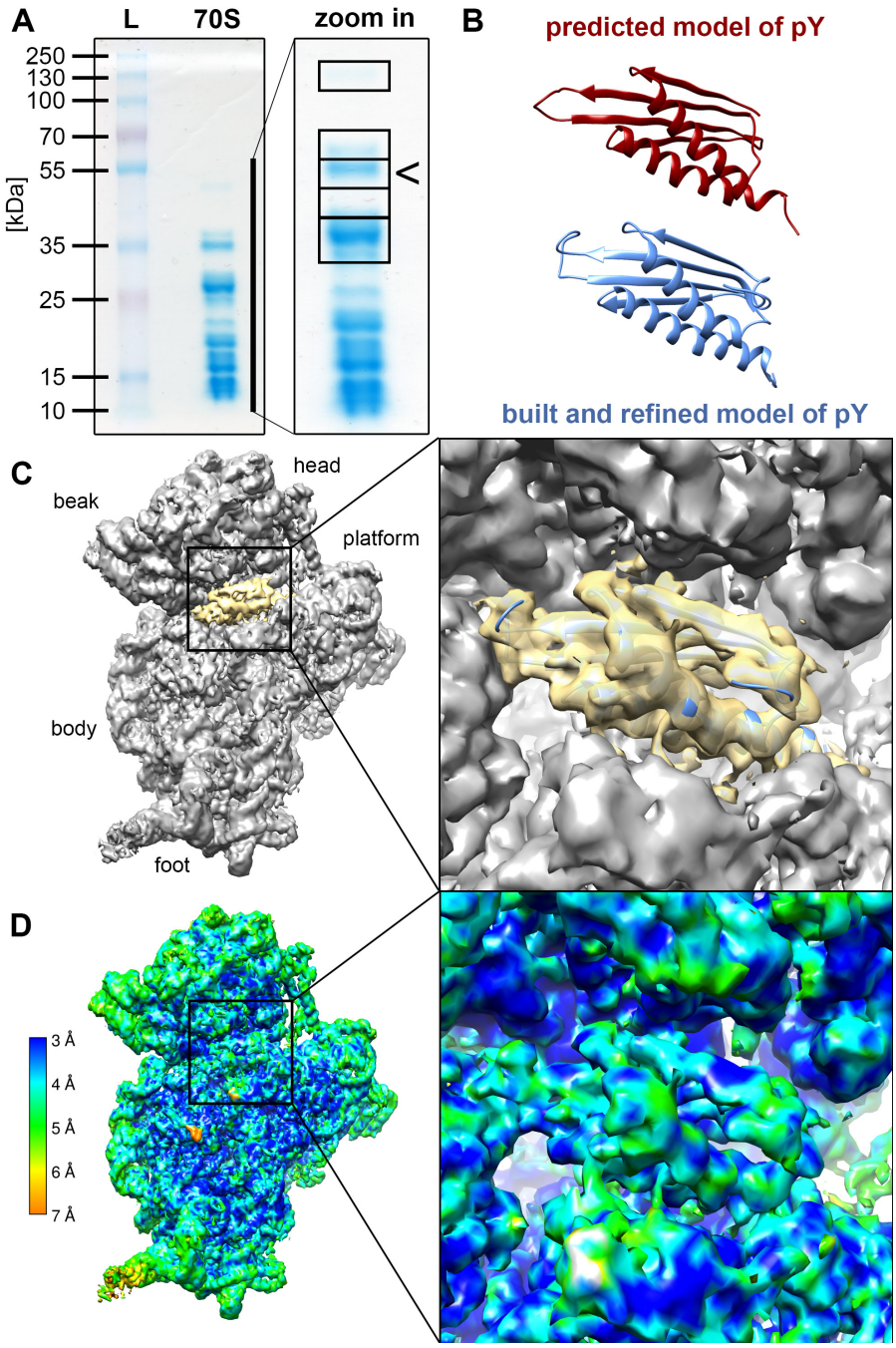

Figure S12. Binding of pY to the chloroplast 70S ribosome. (**A**) Purified chloroplast 70S ribosomes were separated on 12% polyacrylamide gel and stained with Coomassie-Brilliant-Blue. Protein bands in the molecular weight range between 20 and 40 kDa and one band at 50kDa have been cut-out and sent for protein identification by mass spectrometry performed at the Functional Genomic Centre Zurich. Plastid pY (PSRP1), which has a calculated molecular weight of 32kDa, was clearly detected in the slice around 35 kDA (marked by <) with 12 unique peptide hits. (**B**) The C-terminal domain (Accession Code CAA41960.1, residues 75-178) of plastid pY was modelled using Phyre2 (Kelley et al., 2015) and compared with the built and refined structure. (**C**) The density in the mRNA channel can be well-explained by the structure of plastid pY. (**D**) The local resolution plot of the small ribosomal subunit indicates a local resolution range for the density of pY between 3 and 4.5 Å.

Appendix Tables S1-S4

Table S1. Refinement table for the coordinate refinements of the chloroplast 70S ribosome, the 50S large subunit and the 30S small subunit.

Data collection, model refinement, and model validation	30S subunit	50S subunit	70S ribosome
Data collection			
Particles	127‘031	154‘332	140‘583
Pixel size (Å)	1.39	1.39	1.39
Defocus range (μm)	0.8–3.4	0.8–3.4	0.8–3.4
Voltage (kV)	300	300	300
Electron dose (e^-/A^2)	20	20	20
Reciprocal space data			
Spacegroup	P1	P1	P1
a=*b*=*c* (Å)	300.24	300.24	355.84
α=β=γ (°)	90	90	90
Refinement			
Resolution range (Å)	301.26 - 3.65	212.76 - 3.25	252.3 - 3.45
Applied geometry weight (wxc)	1.25	1.25	1.4
No. reflections	1168752	1650858	2296128
R-factor	0.235	0.234	0.246
No. residues			
Protein	2980	3767	6758
RNA	1484	3027	4585
Ligands (Mg^{2+}/Zn^{2+})	185/-	501/2	779/2
B-factors overall	111.6	56.9	90.8
Protein	127.8	67.9	107.0
RNA	100.2	52.1	82.3
Ligands (Mg^{2+}/Zn^{2+})	65.0	22.9	46.4
Validation			
R.m.s. deviations			
Bond lengths (Å)	0.008	0.008	0.008
Bond angles (°)	1.084	1.100	1.066
Molprobity clashscore	10.5	7.7	8.9
Protein			
Ramachandran plot			
Favored (%)	94.9	94.4	94.8
Allowed (%)	4.9	5.3	4.9
Outliers (%)	0.2	0.3	0.3
RNA			
Correct sugar puckers (%)	99.9	99.7	99.7
Backbone conformation outliers (%)	0	0	0

Table S2. Summary of components in the 50S subunit model. The nomenclature of the ribosomal proteins is according to (Ban et al., 2014).

Protein/RNA	Old name	Chain ID	Full size[§] (residues)	Modeled residues	Sequence accession code	Structural homologs	Comments
uL1c	RPL1	-	352	-	CAA54255.1	uL1	not visible
uL2c	RPL2	C	272	19-271	NP_055005.1	uL2	
uL3c	RPL3	D	305	85-305	KNA04906.1	uL3	
uL4c	RPL4	E	293	51-262	KNA22937.1	uL4	
uL5c	RPL5	F	258	39-231	KNA19821.1	uL5	residues 39-52 built as UNK[‡]
uL6c	RPL6	G	305	41-216	KNA14466.1	uL6	
bL9c	RPL9	H	196	42-89	KNA21690.1	bL9	
uL10c	RPL10	I	232	53-189	KNA14105.1	uL10	rigid body fit[†]
uL11c	RPL11	J	224	79-211	CAA39950.1	uL11	rigid body fit[†]
bL12c	RPL12	-	189	-	AAA34031.1	bL12	not visible
uL13c	RPL13	K	250	48-250	AAA34040.1	uL13	
uL14c	RPL14	L	121	1-121	NP_054971.1	uL14	
uL15c	RPL15	M	271	78-262	KNA06817.1	uL15	
uL16c	RPL16	N	135	1-135	NP_054972.1	uL16	
bL17c	RPL17	O	126	11-126	KNA19692.1	bL17	
uL18c	RPL18	P	166	45-166	KNA08833.1	uL18	
bL19c	RPL19	Q	233	116-233	AAF64312.1	bL19	
bL20c	RPL20	R	128	2-120	NP_054958.1	bL20	
bL21c	RPL21	S	256	68-237	CAA40019.1	bL21	residues 68-81 built as UNK[‡]
uL22c	RPL22	T	199	24-195	NP_054974.1	uL22	
uL23c	RPL23	U	198	100-195	Q9LWB5.1	uL23	
uL24c	RPL24	V	192	48-181	KNA06132.1	uL24	
bL27c	RPL27	X	194	66-174	KNA14420.1	bL27	
bL28c	RPL28	Y	148	72-148	KNA16864.1	bL28	
uL29c	RPL29	Z	168	59-159	KNA15596.1	uL29	
bL31c	RPL31	0	130	37-80	KNA12538.1	bL31	50S: 37-80[$]
bL32c	RPL32	1	57	2-49	NP_054985.1	bL32	
bL33c	RPL33	2	66	6-65	NP_054956.1	bL33	Zn^{2+} binding
bL34c	RPL34	3	152	93-152	AAF64157.1	bL34	
bL35c	RPL35	4	159	88-159	AAA34043.1	bL35	
bL36c	RPL36	5	37	1-37	AAF19198.1	bL36	Zn^{2+} binding
cL37	PSRP5	6	142	94-142	KNA26006.1		
cL38	PSRP6	7	116	48-93	AAF64189.1		
23S rRNA		A	2810	2-514, 516-895, 901-1750, 1756-2810	NC_002202.1		Hidden breaks at positions 515 and 1755
5S rRNA		B	121	1-121	NC_002202.1		
4.5S rRNA		W	106	1-106	NC_002202.1		
E-site tRNA		z	mixture of all tRNA species	75-76	from PDB 2J00		CA-3' end of tRNA[*]

§ Full-length protein sequence including putative chloroplast targeting peptide
‡ Unassigned residues were modeled as poly-alanine and deposited as UNK.
† Fold predicted by the Phyre2 protein fold recognition server (Kelley et al., 2015).
$ In the complete 70S model, bL31c bridges the 50S with the 30S *via* a helical linker comprising residues 81 to 91.
* In the 70S structure, an idealized full-length E-site *E. coli* tRNA-Phe (76 residues) from PDB 2J00 was fitted into the density and adjusted prior to minimization.

Table S3. Summary of components in the 30S subunit model. The nomenclature of the ribosomal proteins is according to (Ban et al., 2014).

Protein/RNA	Old name	Chain ID	Full size§ (residues)	Modeled residues	Sequence accession code	Structural homologs	Comments
bS1c	RPS1	8	411		AAA34045.1	bS1	rigid body fit of OB-fold (residues 1001-1068) and extensions (residues 1101-1143, 1201-1263) built as UNK‡
uS2c	RPS2	b	236	4-236	NP_054921.1	uS2	
uS3c	RPS3	c	218	2-217	NP_054973.1	uS3	
uS4c	RPS4	d	201	2-200	NP_054938.1	uS4	
uS5c	RPS5	e	308	122-308	CAA63650.1	uS5	residues 122-150 built as UNK‡
bS6c	RPS6	f	211	99-211	KNA13015.1	bS6	
uS7c	RPS7	g	155	2-155	NP_055001.1	uS7	
uS8c	RPS8	h	134	2-134	NP_054970.1	uS8	
uS9c	RPS9	i	208	65-208	KNA24353.1	uS9	
uS10c	RPS10	j	195	97-195	KNA23234.1	uS10	
uS11c	RPS11	k	138	22-138	NP_054967.1	uS11	
uS12c	RPS12	l	123	2-123	NP_054910.1	uS12	
uS13c	RPS13	m	172	48-157	KNA12871.1	uS13	
uS14c	RPS14	n	100	2-100	NP_054931.1	uS14	
uS15c	RPS15	o	90	16-90	NP_054995.1	uS15	
bS16c	RPS16	p	88	1-80	NP_054914.1	bS16	
uS17c	RPS17	q	165	58-143	KNA21507.1	uS17	
bS18c	RPS18	r	101	21-80	NP_054957.1	bS18	
uS19c	RPS19	s	92	6-83	NP_077750.1	uS19	
bS20c	RPS20	t	183	72-178	¥	bS20	
bS21c	RPS21	u	180	82-146	KNA18384.1	bS21	
cS22	PSRP2	v	260	181-260	AAF64167.1	U1A-type domains	rigid body fit†
cS23	PSRP3	w	179	92-173	AAF64163.1	ycf65	rigid body fit†
bTHXc	PSRP4	x	101	55-94	AAF64154.1	bTHX	
16S rRNA		a	1491	1-1484	NC_002202.1		
bL31c	RPL31	0	130	92-102	KNA12538.1	bL31	30S: 92-102$
plastid pY	PSRP1	y	302	68-183	CAA41960.1	pY	

§ Full-length protein sequence including putative chloroplast targeting peptide.
‡ Unassigned residues were modeled as poly-alanine and deposited as UNK.
† Fold predicted by the Phyre2 protein fold recognition server (Kelley et al., 2015).
¥ At this time, no reference sequence for bS20c of spinach (*Spinacia oleracea*) is deposited in the NCBI nucleotide and protein databases. The sequence of spinach bS20c (Sp_084170_egjy.t1) was identified by BLAST search against the spinach genome (http://bvseq.molgen.mpg.de, (Dohm et al., 2014)) using the bS20c protein sequence of *Beta vulgaris* (XP_010675477.1) as query. The spinach bS20c sequence was aligned against multiple reference sequences of bS20c from higher plants for cross-validation.
$ In the complete 70S model, bL31c bridges the 50S with the 30S *via* a helical linker comprising residues 81 to 91.

Table S4. Intersubunit bridges in the chloroplast 70S ribosome. Bridge: bridge name; type: macromolecules involved (R, rRNA; P, protein); 30S/50S subunit component; rRNA and protein residues forming the bridge.

Bridge	pY bound state (non-rotated state)			difference between states	empty state (rotated state)			Comments
	30S subunit component	50S subunit component	Type		30S subunit component	50S subunit component	Type	
B1a	uS13c: 126-127, 137-138, C-terminus (158-172)†	23S H38 (A-site finger): 896-900 (disordered)	P-R	shift of interaction sites on 30S subunit	-	23S H38 (A-site finger): 896-900 (disordered)	-	H38 of 23SrRNA (A-site finger) is disordered due to the absence of a tRNA in the A-site. Highly conserved arginine residues, R91 and R92 (*E.coli* numbering), of uS13 among bacteria are adapted to I137 and Q138.
	uS19c: 81		P-R		uS19c: C-terminus (79-81)		P-R	
	-		-		16S h30: loop 905-907		R-R	
B1b	uS13c: loop 49-55, 91, 112-113, 115-116	uL5c: 163, loop 189-197, 165-166, 168	P-P	uS13c is shifted by ~20 Å, interaction sites to bL31c lost	uS13c: 115-116 of α-helix (111-128)	uL5c: loop 196-197	P-P	Bridge is conserved. Connecting α-helix of N- and C-terminal domain of bL31c is not resolved at high resolution in the plastid 70S map. Bridge is strongly affected by the SSU head swivelling.
	uS13c: loop 50-53, 102	bL31c: 53, 69, 71	P-P		-	-	-	
B1c	uS14c: 37-38, 41	bL31c: C-terminal α-helix (93-102)‡	P-P	n/a	n/a	Local resolution of the map of the rotated state is too low to identify C-terminal α-helix of bL31c.	n/a	Bridge is conserved with slight changes of some residues involved in the interaction. Interaction of C-terminal α-helix of bL31c is probably maintained based on studies in *E.coli* 70S (Fischer et al., 2015).
	uS19c: 9, 41-42, 64, 67		P-P					
	uS13c: 124		P-P					
	16S h42: 1259-1260		R-P					
B2a/d	16S h44: 1355-1359, 1442-1444	23S H69: 1926-1930, 1933	R-R	stable, no major shifts	16S h44: 1355-1359, 1442-1444	23S H69: 1926-1930, 1933	R-R	Bridge is conserved. Nucleotide sequence and structure of 23S rRNA H69 is conserved. C-terminal domain of uS13c does not contact H69 (similar to E.coli). 16S rRNA h24 and h44 are stabilized by translation factor pY.
	16S h45: 1466	23S H69: 1933	R-R		16S h45: 1466	23S H69: 1933	R-R	
	16S h24: 739, 741	23S H69: 1934-1935	R-R		16S h24: 739, 741	23S H69: 1934-1935	R-R	
B2b	16S h24: 731	23S H68: 1846	R-R	stable, no major shifts	16S h24: 731	23S H68: 1846	R-R	Bridge is conserved.
	16S h45: 1465	23S H71: 1945	R-R		16S h45: 1465	23S H71: 1945	R-R	
B2c	16S h27: 848-849	23S H67: 1841-1843	R-R	shift of interaction site on 30S subunit	16S h24: 719-720	23S H67: 1841-1843	R-R	Bridge is conserved. No Mg2+ ions identified in this area (similar to *E.coli* 70S).
B3	16S h44: 1432-1433, 1367-1368	23S H71: 1961-1964, 1972-1975	R-R	stable, no shifts	16S h44: 1432-1433, 1367-1368	23S H71: 1961-1964, 1972-	R-R	Bridge is conserved. Contacts of uL14c to 16S rRNA h44 is slightly adapted. Bridge B3 is close to pivot point of intersubunit rotation.
	16S h44: 1370, 1372	uL14c: 54, 49	R-P		16S h44: 1370, 1372	uL14c: 54, 49	R-P	

B4	uS15c: 37, 40-41, 53-54, 85, 88, 90	23S H34: loop 724-727	P-R	shift 23S rRNA H34 towards uS15c and away from 16S rRNA h20	uS15c: 37, 40-41, 53-54, 85, 88, 90	23S H34: loop 724-727	P-R	Interactions between uS15c and 23S rRNA H34 are mainly conserved except additional stabilization of the bridge by the C-terminal extension of uS15c interaction with nucleotides 724 and 725 of 23S rRNA H34.
	16S h20: 708-711	23S H34: 728-729	R-R		16S h20: 708-711	23S H34: 728-729	R-R	Additional interaction, which is stabilized in the pY-bound state, between 16S rRNA h20 and 23S rRNA H34 is mediated by Mg^{2+}.
B5	16S h44: 1377-1379, 1422-1424	23S H62: 1722, 1738-1740, 1725, 1736-1738	R-R	stable, no major shifts	16S h44: 1377-1379, 1422-1424	23S H62: 1722, 1738-1740, 1725, 1736-1738	R-R	Bridge is conserved. Bridge B5 is close to pivot point of intersubunit rotation.
B6	16S h44: 1381-1382	bL19c: 228	R-P	stable, no major shifts	16S h44: 1381-1382	uL19c: 228	R-P	Bridge is reduced to a single Arginine residue interacting with minor groove of 16S rRNA h44. Mg^{2+} coordinated.
B7a	16S h23: 650	23S H68: 1856, 1858, 1908	R-R	slight shift of the interaction site on the 23S rRNA	16S h23: 650	23S H68: 1856	R-R	Bridge is conserved.
B7b	16S h23: 628	uL2c:268	R-P	shift of 16S rRNA elements towards 50S subunit	16S h23: 628, 721-722	uL2c: 268, 197-198	R-P	Weak binding according to the density (low threshold applied to see the connection). Elongated distance between interaction partners in comparison to *E.coli* 70S.
B7c	bS6c: loop 160-164	uL2c: loop 131-133	P-P	shift of interaction sites	16S h23: 660	uL2c: loop 133-135	R-P	Plastid-specific loop (160-168) of bS6c interacts with conserved loop (130-132) of uL2c.
B8	16S h14: loop 309-311	uL14c: 13, 96-97	R-P	shift of 16S rRNA elements towards 50S subunit	16S h14: loop 309-311	uL14c: 13, 96, 97, 104, 107	R-P	Bridge is conserved. C-terminus of bL19c is different in comparison to bacterial bL19 and its terminal K233 may interact with 16S rRNA h14.
	16S h14: loop 316-317	bL19c: 160-161	R-P		16S h14: loop 316-318 16S h8: 143	bL19c: 157-161	R-P	

† Residues could not built into the cryo-EM reconstruction and therefore missing in the atomic model.
‡ Only built residues are indicated. Additional C- or N-terminal residues are missing.

Additional References

Bai, X.C., Rajendra, E., Yang, G., Shi, Y., and Scheres, S.H. (2015). Sampling the conformational space of the catalytic subunit of human gamma-secretase. Elife *4*.

Ban, N., Beckmann, R., Cate, J.H., Dinman, J.D., Dragon, F., Ellis, S.R., Lafontaine, D.L., Lindahl, L., Liljas, A., Lipton, J.M.*, et al.* (2014). A new system for naming ribosomal proteins. Curr Opin Struct Biol *24*, 165-169.

Dohm, J.C., Minoche, A.E., Holtgrawe, D., Capella-Gutierrez, S., Zakrzewski, F., Tafer, H., Rupp, O., Sorensen, T., Stracke, R., Reinhardt, R.*, et al.* (2014). The genome of the recently domesticated crop plant sugar beet (Beta vulgaris). Nature *505*, 546-+.

Fischer, N., Neumann, P., Konevega, A.L., Bock, L.V., Ficner, R., Rodnina, M.V., and Stark, H. (2015). Structure of the E. coli ribosome-EF-Tu complex at <3 A resolution by Cs-corrected cryo-EM. Nature *520*, 567-570.

Greber, B.J., Bieri, P., Leibundgut, M., Leitner, A., Aebersold, R., Boehringer, D., and Ban, N. (2015). Ribosome. The complete structure of the 55S mammalian mitochondrial ribosome. Science *348*, 303-308.

Kelley, L.A., Mezulis, S., Yates, C.M., Wass, M.N., and Sternberg, M.J. (2015). The Phyre2 web portal for protein modeling, prediction and analysis. Nat Protoc *10*, 845-858.

Noeske, J., Wasserman, M.R., Terry, D.S., Altman, R.B., Blanchard, S.C., and Cate, J.H. (2015). High-resolution structure of the Escherichia coli ribosome. Nat Struct Mol Biol *22*, 336-341.

Yusupov, M.M., Yusupova, G.Z., Baucom, A., Lieberman, K., Earnest, T.N., Cate, J.H., and Noller, H.F. (2001). Crystal structure of the ribosome at 5.5 A resolution. Science *292*, 883-896.